Outer rotor wound field flux switching machine for In-wheel direct drive application

Naseer Ahmad[1] ✉, Faisal Khan[1], Hazrat Ali[1], Samra Ishaq[1], Erwan Sulaiman[2]

[1]Electrical Engineering, COMSATS University Islamabad, Abbottabad Campus, Abbottabad, Pakistan
[2]Electrical Engineering, Universiti Tun Hussein Onn Malaysia, Locked Bag 101, BattuPahat, johor, 86400 Malaysia, Malaysia
✉ E-mail: n.ahmadmwt@gmail.com

Abstract: Nowadays the flux switching machines offer pivotal role in high speed applications. The flux sources (field excitation coil and armature winding or permanent magnet) are confined to the stator leaving rotor completely passive, and thus making the flux switching machine (FSM) more suitable for industrial applications. This paper emphasizes salient rotor pole and non-overlapping windings embedded in electrical machine design possess some pertinent features such as reduced copper losses, low-cost, and usage in high speed applications. The proposed design is analyzed for coil test analysis and flux linkage and torque. On the basis of the analysis performed, it is clear that 12-slot/13-pole has low cogging torque, high flux linkage, and maximum torque, compared with other topologies of outer rotor field excitation FSM. A deterministic optimization technique is adopted to enhance the performance of 12-slot/13-pole design. Further, finite element analysis (FEA) results are verified through Global Reluctance Network (GRN) methodology, which show close resemblance with error less than 1.2%. Hence, it validates the proposed design for outer rotor field excitation FSM direct drive application. The proposed design for hybrid electric vehicle torque characteristic is compared with existing interior permanent magnet synchronous machine (IPMSM) and 6-slot/7-pole wound field flux switching machine (WFFSM).

1 Introduction

With the increase in population of the world, demand for personal vehicles is continuously increasing. The increase in the demand of vehicle causes global warming and green house effects. Internal combustion engine has drastic effects on the environment. According to report published in 2008, it was observed that in the year 2000, a seven percent of CO_2 was emitted from vehicles. Besides, due to industrial expansion, the expected increase in CO_2 was reported to have been twice by 2015 [1]. Internal Combustion Engine (ICE) vehicles contribute significantly to radiation emission as well as inefficient fuel consumption. Hence, electric vehicle powered by a battery is the best solution to the problem of energy crisis and global warming, as electric vehicle has no radiation emission and no oil consumption [2, 3]. Nowadays, research trends in Electric Vehicles (EV) and Hybrid Electric Vehicles (HEVs) are the developments on more efficient energy systems. The most important component for electric vehicle drive system is an electric motor with high power density, high torque, and constant power at different speed characteristics.

Successfully installed machines in HEVs are Induction Machines (IMs), Switch Reluctance Machines (SRMs), DC machines and Permanent Magnet Synchronous Machines (PMSMs).

Induction machines have low cost, high reliability, low maintenance, and rugged structure, and can be employed in electric vehicle drive system. However, disadvantages of induction machines (IMs) include low power factor, high losses, low usage-factor for inverter, and low efficiency.

DC machines require large structure, having low efficiency and low reliability. Due to these features, DC machines are unfavourable for HEVs. SRM has robust structure and no permanent magnet but the use of SRM causes problems of acoustic noise generation and ripples in high torque [4]. PMSMs have high torque and better efficiency but they have demerits of demagnetization, complex structure which is difficult to optimize and permanent magnet cost issues.

The PM machines have high efficiency and high torque density. However, application of PM machines is limited by high cost of rare earth magnets. Secondly, the operation of flux-weakening at high-speed is difficult to achieve due to PM excitation method. To overcome the aforementioned issues, the design of hybrid excitation flux switching machine (HEFSM) was proposed. In HEFSM, all the active components are placed on the stator while rotor structure is robust having a salient passive part. The hybrid excitation is an association of permanent magnets and a wound exciter suitable for high-speed applications in which advantage of both the PM machine and the DC synchronous machine are combined [5]. HEFSMs have the ability to enhance power density, torque, efficiency, flux weakening performance and variable flux capability [6].

The PM is substituted by DC excitation coil in field excitation flux switching machine (FEFSM) for further reduction of cost as compared to HEFSM [7]. The design of low cost single phase FEFSM has been suggested for automobiles industry [8]. The power density of single phase FEFSM was higher than the universal equivalent induction machines and both the designs have almost same efficiency. However, problems associated with single phase FEFSM are large ripples in torque, low starting torque and fixed revolving direction [8]. To overcome the deficiencies related to the single phase FEFSM, three-phase FEFSM was proposed in which PM was completely removed and field excitation coil (FEC) was housed on the stator. Higher torque and power density are the key features of three-phase FEFSM, having relatively simpler structure [9]. As in FEFSM, all the active parts are present on the stator, thus providing easy cooling mechanism, while at the same time, field excitation provides the controllable flux with the variable flux capabilities [10, 11]. In summary, outer rotor has edge over inner rotor providing advantages to completely eliminate drive belts, mechanical transmission, and differential gears. Moreover, high efficiency of outer rotor, increased space in vehicle, and weight reduced [12]. FEFSM with non-overlap and overlap windings have been investigated and comparisons of results show that overlapped winding of FEFSM has better characteristics [13]. Thus, FEFSM is a good candidate for the electric propulsion system of HEVs with lower cost and simple design structure.
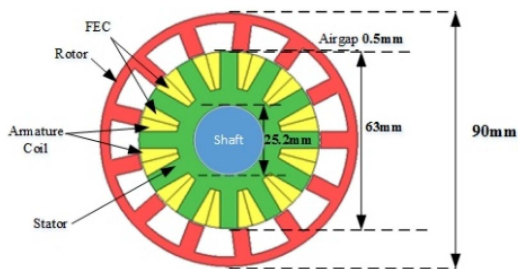
Fig. 1 *Outer rotor FEFSM*

Table 1 Design Parameters [13]

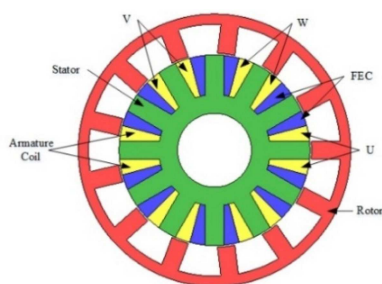| Geometry design parameter	Value
stator slot number	12
rotor poles	5, 7, 8, 10, 11, 13, 14
rated speed (rpm)	400
number of turns in fec and armature winding	180
split ratio	0.7
width stator tooth (mm)	6.2
outer radius (mm)	45
back-iron thickness of stator (mm)	3.4
width of rotor pole (mm)	5.8
axial length (mm)	25
steel	35H210
axial length (mm)	25

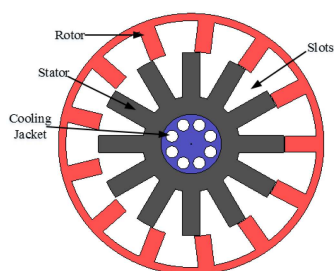**Fig. 2** *Three Phase 12-Slot/13-Pole outer rotor FEFSM*

Fig. 3 *Cooling jacket of outer rotor FEFSM*

This paper presents the three-phase outer rotor FEFSM employing salient rotor pole with seven different rotor pole topologies. The proposed design offers novelty in the outer-rotor and the non-overlapping windings for high speed applications. The various performance analysis are examined by 2D FEA. The proposed design flux linkage verified through GRN and employs deterministic optimization in enhancement of power, torque, and efficiency compared to existing IPM and 6-slot/7-pole WFFSM.

The rest of the paper is organized as follows: Section 2 provides three phase outer rotor FEFSM pole study. Section 3 2D FEA based initial design performance analysis discusses. Section 4 have detailed discussion om optimization and validation through GRN. Section 5 provides optimized design analysis and Section 6 have a torque comparison with existing design. Section 7 discuss the efficiency and loss analysis. Finally, the paper is concluded in Section 8.

2 Three phase outer rotor FEFSM rotor pole study

As in FSM the flux sources are only housed to stator, while rotor is completely free from winding, thus acclimating it suitable for high speed applications. The rotor position determines the basic operating principle of FEFSM, as the flux linkage could be negative or positive with respect to the rotor position. To determine number of various rotor poles as in (1).

$$N_r = N_s \left(1 \pm \frac{K}{2q} \right) \qquad (1)$$

Where N_r is rotor pole number, N_s is stator slot number, and q is number of phases. Seven different topologies have discussed in [14]. The cross-sectional view of machine is shown in Fig. 1 and Table 1 are summarized design parameters. All the design topologies have a rotor robust structure and non-overlapping windings.

2.1 Initial design specification

The design detail and specification of the proposed outer rotor FEFSM geometry is shown in Fig. 2. In the proposed design, some assumptions have been made, which are: (a) slot area of armature coil and slot area of FEC must be constant and in a trapezoidal shape. (b) split ratio is between 60 to 70%. (c) for high speed and high torque, the widths of rotor tooth and stator tooth play a vital role as in (2) [15].

$$\sum \text{width of stator tooth} = \sum \text{width of rotor tooth} \qquad (2)$$

The number of turns of FEC and armature coil for can be determined by in (3) and in (4).

$$J_a = \frac{I_a N_a}{\alpha S_a} \qquad (3)$$

$$J_e = \frac{I_e N_e}{\alpha S_e} \qquad (4)$$

Where, I, α, N, S, and J are current, filling factor, number of turns, area of the slot, and current density respectively and subscript 'a' and 'e' represents armature and Field coil respectively.

Thermal management system is essential for outer rotor FSM design. High temperature rise can damage aging\insulation effect, increasing copper losses with increasing winding temperature, and fault occurring in machine. Cooling jacket concept is proposed for thermal management as shown in Fig. 3. Mainly three types of techniques are radation, convection, and conduction. In this design, water is selected as cooling medium. The tempature of water can not increase because water enter from one side and out from other side. Major part of heat absorbed be the coolent medium and some of the part of heat will be flow through convection to air [16]. Water jacket cooling system is available for maximum current density of 30 A/mm^2.

## 3 2D-FEA based initial design performance analysis

Typically, 2D- FEA solver is used for the design and analysis of outer rotor FEFSM. Rotor, stator, armature coil and field coil are drawn in geometry editor and then link with J-MAG designer for further analysis. The main objective of this paper is to design robust and efficient outer rotor structure, non-overlapping windings, low cost, and highly efficient motor. Following analysis for proposed design has been performed using 2D-FEA solver.

3.1 Coil arrangement test and flux linkage

The coil arrangement test is used to investigate the flux linkage in every armature coil slot and verify the basic operating principle of outer rotor FEFSM for applications in HEV. The analysis of

a

b
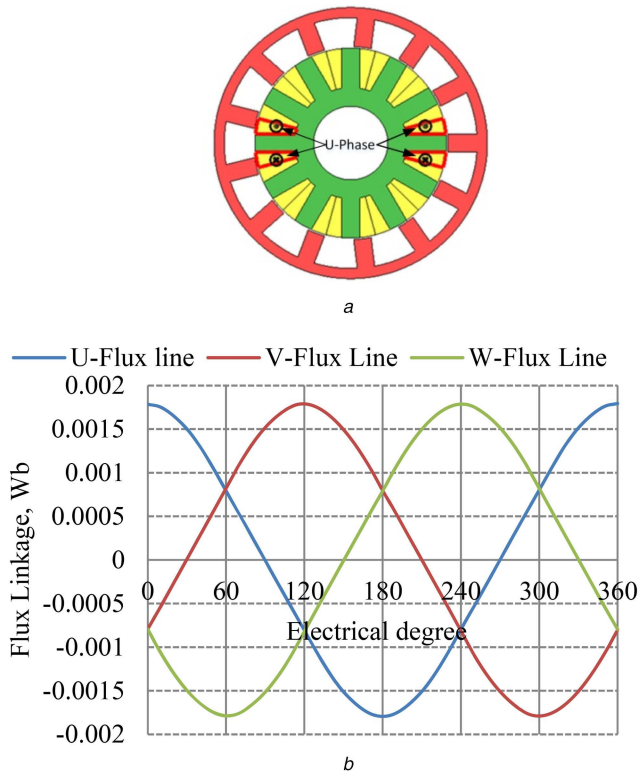
Fig. 4 *Odd rotor pole configuration*
(a) U-Phase of odd rotor pole, *(b)* Flux linkage of odd rotor pole
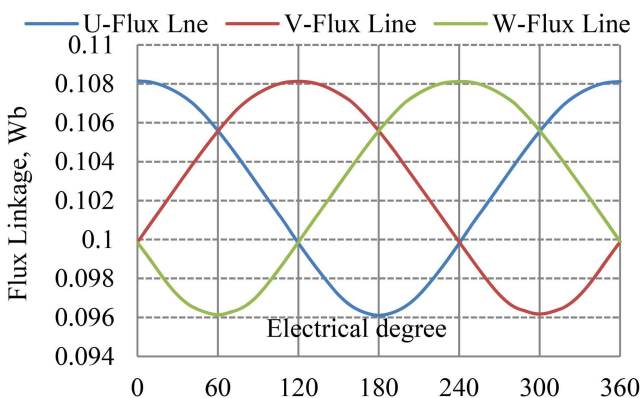
Fig. 5 *Even rotor pole flux linkage with opposite coil combination*

magnetic flux linkage is performed through the coil test at no load condition.

The odd and even rotor pole winding configuration is different in outer rotor pole FEFSM as shown in Figs. 4*a* and *b* respectively. The odd rotor pole winding is arranged such that the opposite coils are combined resulting in bipolar flux linkage as show in Fig. 4*b* while unipolar flux linkage for similar configuration winding in even rotor pole.

The flux is also shifted above from zero level as illustrated in Fig. 5. This issue of flux shifting above zero level is addressed by combining alternate coil pole pair as shown in Fig. 6*a*. As a result, bipolar in flux linkage and attains zero level as depicts in Fig. 6*b*.

Table 2 shows the magnetic flux linkage for various topologies of outer rotor FEFSM at 400 rpm speed and analysis seven different rotor pole of outer rotor FEFSM with fixed stator slots. Table 2 shows that the 7-pole and 11-pole design has the maximum peak of 0.00204Wb, and their performances were relatively enhanced than other designs. The designs having odd rotor poles are not preferred over the even rotor pole due to their unbalanced magnetic force.

3.2 Torque

At no-load analysis torque is cogging torque. The cogging torque causes vibration and noise in operation of the machine. Table 2 shows that magnitude of cogging torque is maximum for 5-pole, 8-pole, and 14-pole topologies while it is minimum for 11-pole and 13-pole and the highest peak-to-peak cogging torque is about 0.4 Nm of 5-pole. The 13-pole have lowest cogging torque that produce less noise and vibration. The best topology is selected based on the lowest cogging torque. Minimizing cogging torque with different techniques like pole pairing, skewing, chamfering, and notching.

Fig. 7 shows the relation between various armature current density (J_a) curves and torque at same field current density (J_e) which describes the direct relation between torque and armature current density. The armature current density is changed from 0A/mm^2 to 20A/mm^2 and field current density is kept constant at 20A/mm^2. The design is simulated at various current densities and the average torque is examined accordingly. The average torque of 12slot-13pole is 0.687 Nm, maximum among all topologies.

4 Optimization procedure

The proposed 12-slot/13-pole outer rotor FEFSM is optimized to enhance the torque characteristic. The initial torque achieved is 88.04 Nm, while the target torque 138 Nm.

To achieve better performance, the rotor and stator parts have design parameters S1 to S7, as shown in Fig. 8*a*. S1 and S2 are the rotor parameters, S3 is the radius of the stator, S4 is back iron of stator, S5 and S6 are the stator poles width, and S7 is armature coil parameter. Whereas, S1 and S2 are the depth and width of rotor pole, respectively. Deterministic optimization technique (single variable optimization) is applied to achieve targets requirements [4]. In deterministic optimization technique, the air gap and slot area of armature coil and FEC are kept constant while a free parameter is changed. Firstly, change the rotor parameters S1 and S2 while keeping all free parameters of the stator constant. In order to accomplish maximum torque, rotor pole depth, S1 and rotor pole width, S2 are changed while other parameters are kept constant. Moreover, S3 is the most dominant parameter for attaining maximum torque and is updated as follows. Increasing the stator radius S3 will result in increasing the stator back iron length S4, while keeping armature slot area S7 and FEC slot area S6 constant. Once the maximum torque is achieved, the stator radius S3 and S4 are kept constant and S5, S6 and S7 are changed. Similarly, the optimal S5 value is also kept constant and S6 is updated. The torque improvements are shown in Fig. 8*b*.

The initial and final design parameters are summarized in Table 3. The design optimization process and modification is iterated until maximum torque performance is achieved. After optimization process, the structure difference between initial and final design is illustrated in Fig. 9. Moreover, the armature slot of final design has 29.93% higher depth than FEC slot to produce optimal magnetic flux. Table 4 represents different performance of all rotor pole after applying optimization and 12-slot/13-pole configuration is best combination among all topologies.

Maximizing average torque and minimizing cogging torque are the objective functions of optimization represented in (5) and to set constrain for higher average torque value and cogging torque should be lesser, as represented in (6).
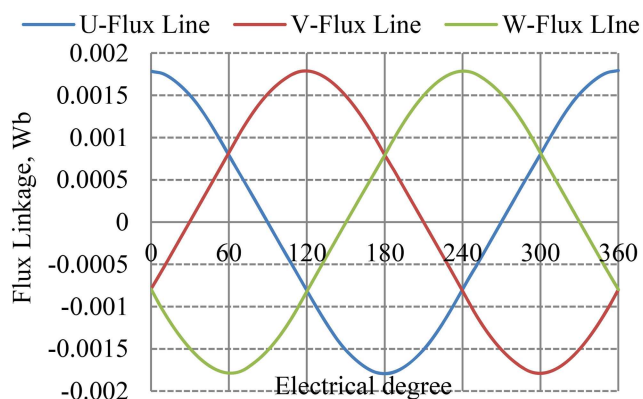
- Objective functions:

$$\begin{array}{l} \text{Maximizing average torque} \\ \text{Minimizing cogging torque} \end{array} \qquad (5)$$

- Constrains:

$$\begin{array}{l} \text{Average torque} \ \leq 138\,\text{Nm} \\ \text{Cogging torque} \ \leq 10\% \text{ of } T_{\text{max}} \end{array} \qquad (6)$$
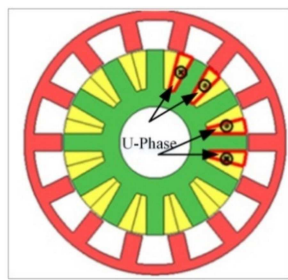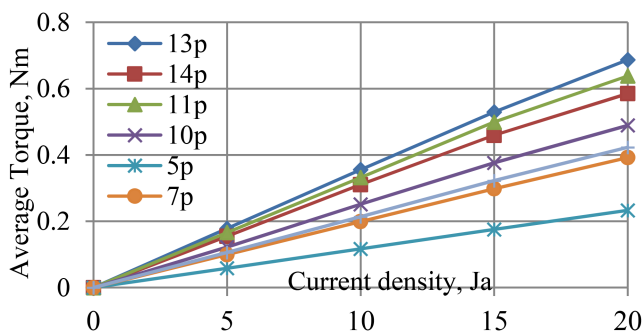
a

b

Fig. 6

(a) Even rotor pole coil combination, *(b)* Flux linkage of Even rotor pole coil combination

Fig. 7 *Average torque vs. current density (A/mm²)*

Table 3 Optimization parameters and comparison

| Design parameter	Initial	Final	IPM	WFFSM
number of stator slot	12	12	48	6
number of rotor pole	13	13	8	7
axial length(mm)	50.8	50.8	50.8	132
rotor outer diameter(mm)	132	132	132	50.8
air gap(mm)	0.73	0.73	0.73	0.73
split ratio	0.7	0.82	0.61	0.66
stator tooth width(mm)	20	24	7.3	33.5
back iron(mm)	9	10	20.2	17.5
rotor pole arc(degree)	—	—	—	21.0
rotor pole width	18	20	—	—
speed	1200	1200	1200	—
max. DC-bus voltage inverter	—	650 Vrms	650 Vrms	—

4.1 Validation through magnetic equivalent circuit (MEC)

Reluctance networks of 12slot/13pole outer rotor FEFSM with air gap MEC modules corresponding to different rotor positions and MEC modules of both rotor and stator are combined as GRN. Air gap MEC module is varying corresponding to the rotor position. Consequently, the different MEC modules are determined in
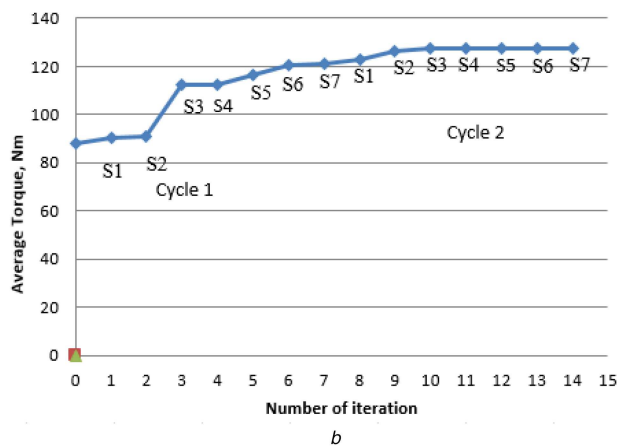
Table 2 Flux linkage and cogging torque

Performance	5 pole	7 Pole	8 pole	10 pole	11 pole	13 pole	14 pole
flux linkage	20.6	20.4	18.1	16.6	20.4	19	14
cogging torque	0.4	0.08	0.09	0.112	0.04	0.04	0.2

all values of flux linkage are multiplied by 10^{-4} and unit is Wb. Unit of cogging torque is Nm.
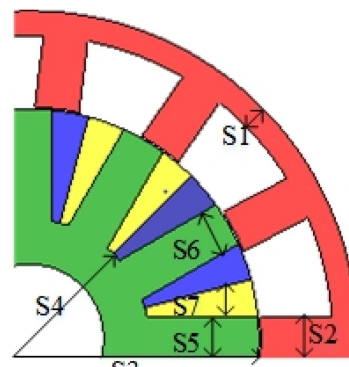

a

b

Fig. 8

(a) Design parameter for optimization, *(b)* Average torque effect on different parameters

accordance with rotor position. To reduce the computational time and complexity, stator section of 12slot/13pole outer rotor FEFSM is divided into five segments. Different air gap MEC modules are observed when the rotor changes position corresponding to stator segments. The computational complexity and time should be avoided, half machine of MEC is modelled under different interval corresponding to position of rotor. Flux distribution of air gap mainly contributes to performance of outer rotor FEFSM, as mainly electrical machine energy converted in this part of machine. every MEC modules occurs after five intervals thus minimizing varieties of GRN [17]. Flux tube in air gap changes with changing rotor position, as a result concentration of flux and permeance of flux tube also varies. Different combinations of air gap MEC modules corresponding to various rotor positions are examined, which represent the changes in air gap flux distribution.

Magnetic flux distribution in the air gap is highly sensitive to the rotor position. Shifting scheme for 12slot/13pole outer rotor FEFSM is determined. Shifting scheme of proposed machine investigates the MEC modules in terms of matrices and GRN of the proposed machine is obtained by combining these matrices.
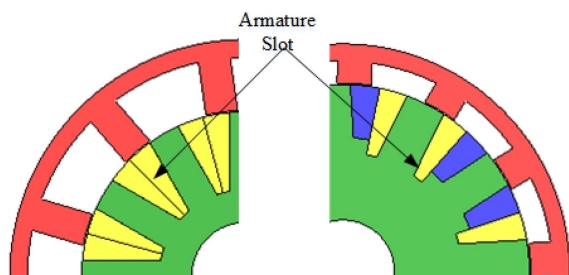
Fig. 9 *Comparison of initial and final design*

Table 4 Optimized performance

| Different rotor pole	Flux linkage, Wb	Cogging torque, Nm Un-optimized	Optimized	Torque, Nm	Power, kW
12-slot\5-pole	0.27	25	20	33	1.65
12-slot\7-pole	0.25	18.1	12.36	39	1.95
12-slot\10-pole	0.30	21.12	16.04	75.1	3.4
12-slot\11-pole	0.31	17.5	11.1	114.3	4.6
12-slot\13-pole	0.33	16.01	9.4	132	5.7
12-slot\14-pole	0.198	24.07	17.3	89.7	3.9
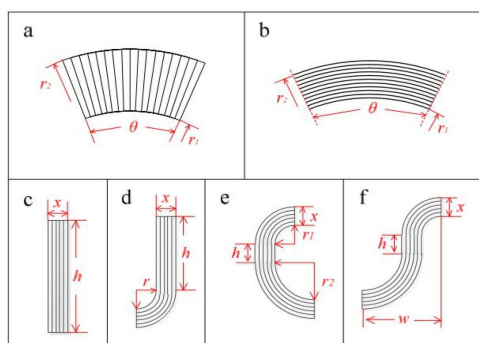
Fig. 10 *Flux tubes*
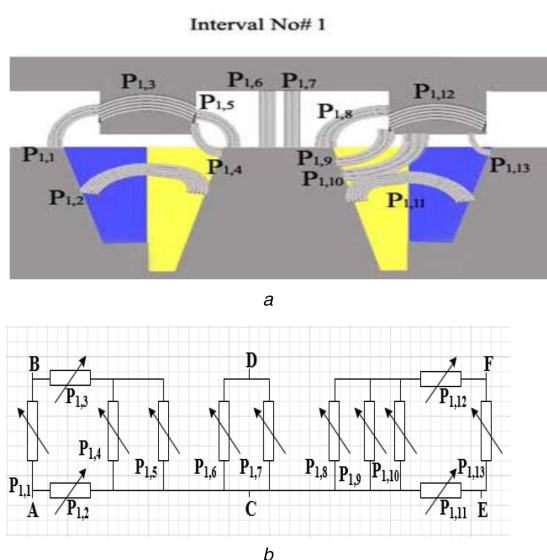
Fig. 11 *Interval 1*
(a) Flux tubes for interval 1, *(b)* MEC

Table 5 Formulas for permeances of flux tubes [18]

flux tubes	Permeance (P)	Flux tubes	Permeance (P)
a	$\dfrac{\mu L\theta}{\ln\left(\frac{r_2}{r_1}\right)}$	d	$\dfrac{2\mu L \cdot \ln\left(1 + \frac{\pi x}{\pi r + 2h}\right)}{\pi}$
b	$\dfrac{\mu L\ln\left(\frac{r_2}{r_1}\right)}{\theta}$	e	$\dfrac{\mu L \cdot \ln\left(1 + \frac{2\pi x}{\pi r_1 + \pi r_2 + 2h}\right)}{\pi}$
c	$\dfrac{\mu L x}{h}$	f	$\dfrac{2\mu L x}{(\pi w + 2h)}$
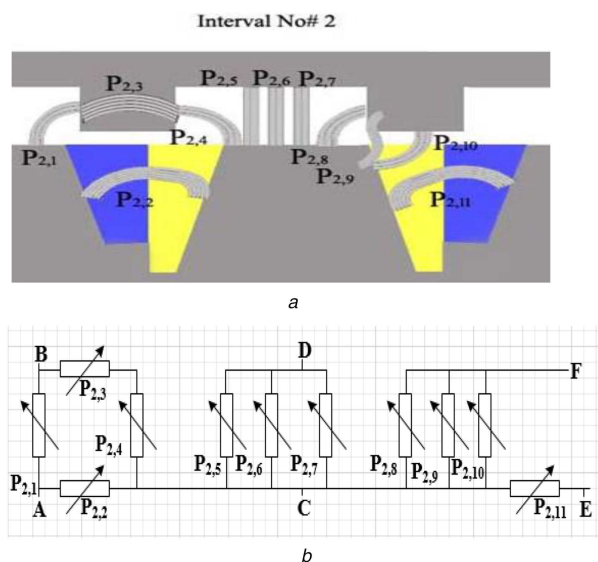
Fig. 12 *Interval 2*
(a) Flux tubes for interval No. 2 and, *(b)* MEC

4.2 Airgap MEC modules

FEA on 12slot/13pole outer rotor FEFSM is performed to model air gap magnetic flux distribution when rotor tooth travels in different segments. Refer to Table 5, A, dA, L, and μ are head face of flux tube, surface element on the head face, total length of a flux line originated from one face element, and permeability of the material, respectively. Both L and μ can change over surface A. The six kinds of flux tubes and their permeance calculating equations are shown in Fig. 10 and Table 5 respectively. The equally distributed flux lines are directed along X-axis while the homogeneously assumed magnetic properties of every flux line is directed along Y-axis. The permeance of flux tubes shown in Figs. 10*a* and *b* are calculated through cylindrical coordinate system in order to minimize computational complexity while, flux tubes permeance are calculated through cartesian coordinate system as shown in Figs. 10*c–f*.

FEA are grouped into certain number of flux tubes as shown in Fig. 11*a* (interval 1), Fig. 12*a* (interval 2), Fig. 13*a* (interval 3), Fig. 14*a* (interval 4) and Fig. 15*a* (interval 5).
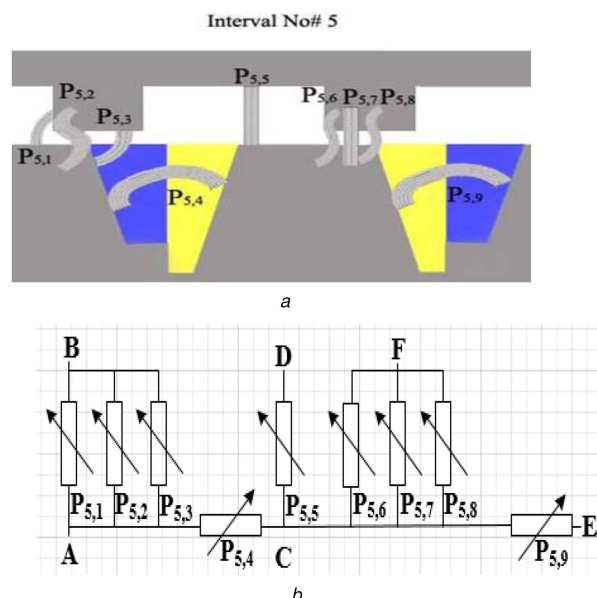
Fig. 10 represents different types of flux tubes selected from Table 5 for permeance calculations. Five different airgap MEC modules with variable permeances are shown in Fig. 11*b* (interval 1), Fig. 12*b* (interval 2), Fig. 13*b* (interval 3), Fig. 14*b* (interval 4) and Fig. 15*b* (interval 5).
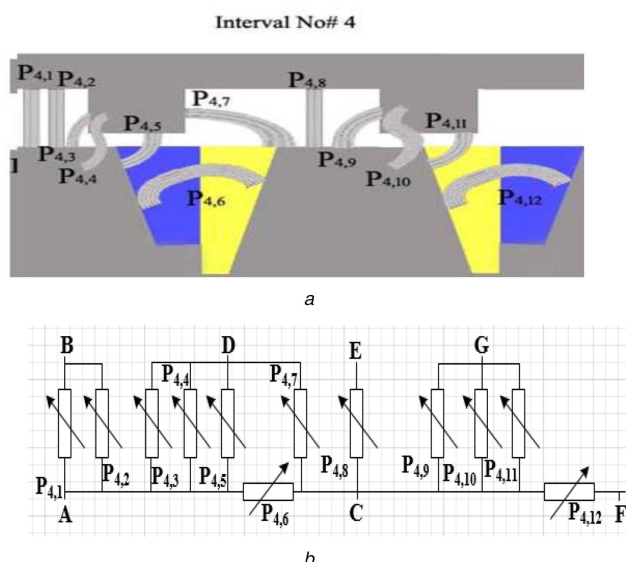
4.3 Validation of FEA through GRN

Accuracy of GRN methodology and nonlinear MEC models for 12slot/13pole outer rotor FEFSM is verified by comparing FEA results with corresponding no-load U-phase flux linkage. Fig. 16 shows GRN. Geometric dimensions and magnetic parameters of 12slot/13pole outer rotor FEFSM are shown in Table 1. Comparison of no-load U-phase flux linkage calculated form FEA and GRN methodology is presented in Fig. 17. Results achieved from GRN methodology clearly resembled with FEA with errors
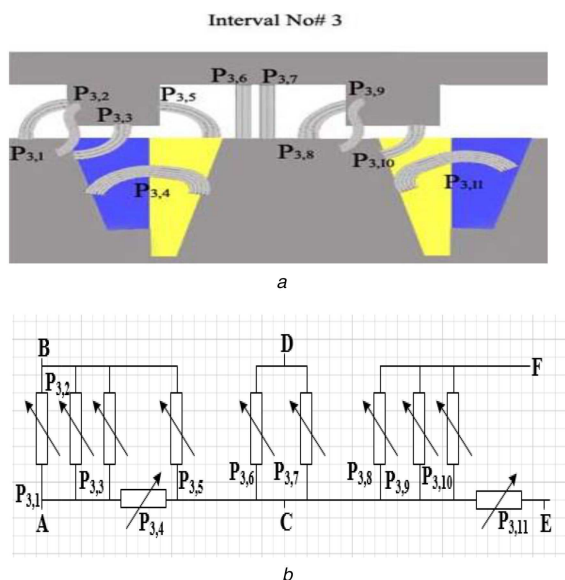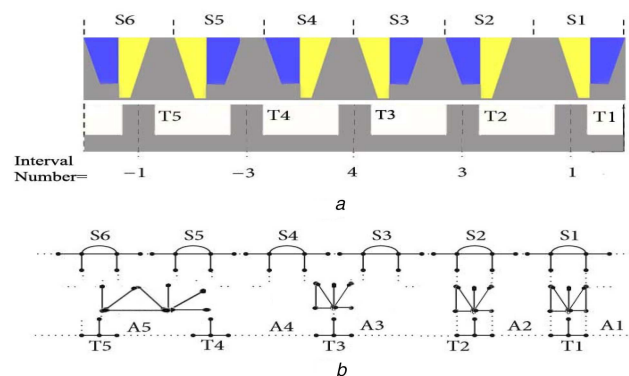
Interval No# 3

Fig. 13 *Interval 3*
(a) Flux tubes for interval No. 3 and, *(b)* MEC

Interval No# 4

Fig. 14 *Interval 4*
(a) Flux tubes for interval No. 4 and, *(b)* MEC

less than ~1.2%. Hence the 12slot/13pole outer rotor FEFSM results are validated through GRN methodology.

5 Optimized design analysis

In contrast to refined design, an increased torque and power for outer rotor FEFSM with updated parameters are achieved through deterministic optimization techniques as shown in Fig. 18. After 3 optimization cycles, the accomplished power is 5.69 kW while the achieved torque is 132.513 Nm. For the optimized turns, the applied FEC and armature current are kept fixed while the number of turns is altered to achieve the target power. The impact of different combinations of turns on power and torque is evaluated in Fig. 19.

Fig. 19 show that increasing number of turn torque profile is linearly increased up to 310 number of turns and after 310 number of turns torque is reduced due to saturation effect. Due to number of turn optimization, torque is increased by 1.4 percent. It is clear from Fig. 19 that high average power is achieved at 290 turns. For higher number of turns, the copper losses are increased.

The number of turns selected to investigate the efficiency of optimal design is 310, in order to achieve the target power and torque values. Table 3 summarizes various initial and final design parameters. In contrast to the initial design, the slot area is

Interval No# 5

Fig. 15 *Interval 5*
(a) Flux tubes interval No. 5 and, *(b)* MEC

Fig. 16 *Global MEC of 12S-13P ORFEFSM*

increased for a high number of turns. Fig. 20 shows the torque and power relationship with armature current density J_a. With increasing armature current density J_a, an increased linearly torque profile is observed in the graph. The torque value is also further increased when increasing armature current density J_a. Behind 30 A/mm^2 increase in armature current density J_a that caused decreased in power due to saturation effect, copper losses increasing, and high temperature effect. The optimal torque for final design is 132.513 Nm, which is 31.8% increase compared to the initial design.

6 Torque comparison

Fig. 21 illustrates the torque versus armature current density (J_a) curves keeping field current density (J_e) constant. The outer rotor FEFSM achieved a torque of 132.5 Nm at J_a and Je of 30 A/mm^2. The torque profile shows linear behaviour by increasing the armature current density. Fig. 21 compares outer rotor FEFSM torque characteristic with IPM and 6-slot/7-pole WFFSM.

Internal Permanent Machine (IPM) is successfully installed and commercialized for HEV's by the Toyota Prius company. The performance parameter of IPM and 6-slot/7-pole WFFSM are published in [12]. These two machines are considered as a bench mark. A 6-slot/7-pole WFFSM is relatively the best machine compared with other machines because of high torque density. This machine achieves approximately 60% torque density of IPM at same current density. Fig. 21 shows the average torque versus current density for IPM and 6-slot/7-pole WFFSM machine [13].
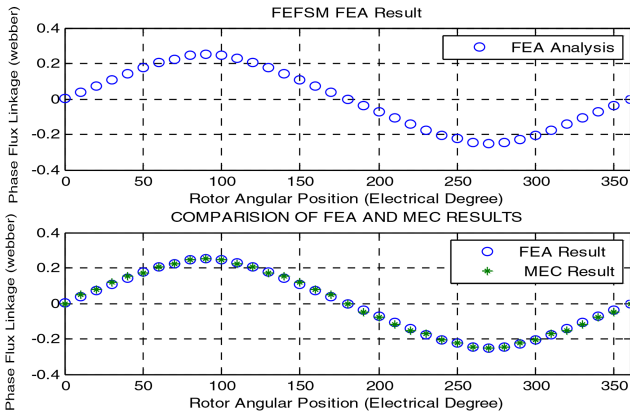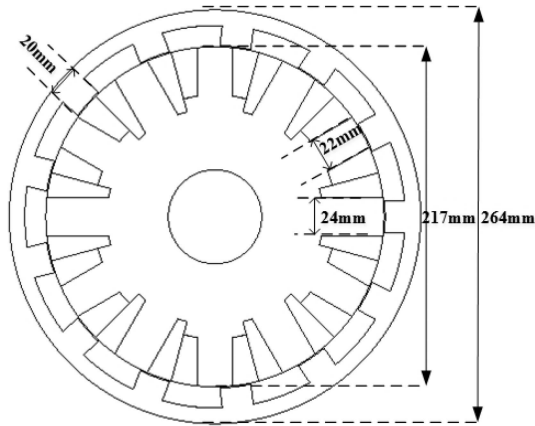
Fig. 17 *Combine FEA and MEC*

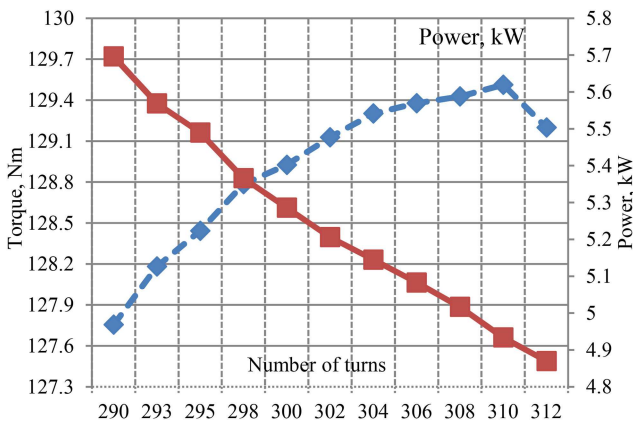**Fig. 18** *Optimized design of 12slot\13pole ORFEFSM*

Fig. 19 *Torque and power versus number of turns*

The average electromagnetic torque, T_e, generally consist of an excitation torque, T_{ex}, and reluctance torque, T_{rl}, and expressed for multiphase arrangement as [19].

$$T_e = \sum_W T_{rl,W} + \sum_W T_{ex,W} \qquad (7)$$

$$T_e = \frac{1}{2} \sum_W i_W^2 \frac{dL_W}{d\theta} + \sum_W i_W \frac{d\Psi_{ex}}{d\theta} \qquad (8)$$

Where L_W, i_W, θ, and Ψ_{ex}, are the inductance of phase winding, phase current, electrical degree of rotor position, and due to field excitation flux linkage and V, U, W are the phase designation.

The total torque produces due to excitation torque, T_{ex} where T_{rl} is negligible contribution. As further, general expression as,
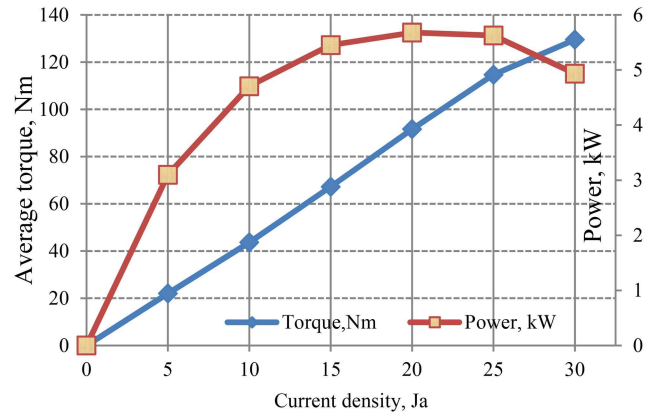

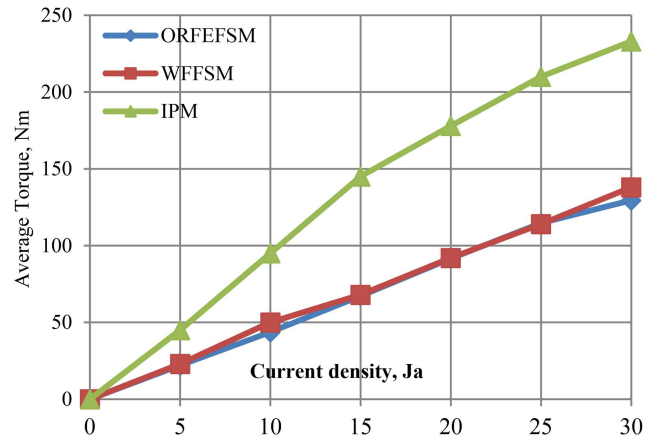**Fig. 20** *Power and torque versus armature current density*

Fig. 21 *Comparison of torque*

$$T_e = \frac{P_i(t)}{\omega_r} = \frac{\sum_W e_W(t) i_W(t)}{\omega_r} \simeq \sum_W T_{ex,W} \qquad (9)$$

Where ω_r, P_i, and e_W are the rotating speed, instantaneous power, and back EMF. One of the best advantages of FSM is the control the average electromagnetic torque by both armature and field current.

The proposed motor 12-slot/13-pole outer rotor FEFSM is optimized to acquire maximum average torque. For performance, the comparison makes 12-slot/13-pole motor similar size as IPM machine. Fig. 21 shows that inner and outer rotor FSM have same result up to 25 A/mm². Fig. 21 shows that 12-slot/13-pole outer rotor FEFSM can achieve average torque approximately 57% of IPM and 95% of 6-slot\7-pole WFFSM.

7 Stress analysis

The rotor stress analysis is very important for high speed machines. It is identifying the optimal rotor tensile strength at different speeds. Beyond the maximum stress the rotor structure will breaks. Rotor stress analysis is a technique to identify the principal stress, nodal force and displacement occurred in the rotor structure in an ideal state after load is applied. Generally, condition for mechanical stress of the rotor structure is accomplished by centrifugal force due to the longitudinal rotation of rotor. Additionally, centrifugal force of the rotor is greatly affected with the speed. Rotor could highly withstand to the stress, if the principal stress of the rotor is higher. Principal stress is a crucial result in the analysis of stress. With increasing the angular velocity of the rotor principal stress is increased exponentially. 35H210 steel is used for outer rotor WFFSM, which have a maximum tensile strength is 500 MPa. Fig. 22 shows stress analysis at various speed. At 15,000 rpm rotor maximum stress is 263 MPa, which shows that it can rotates without any deformation at high speed.
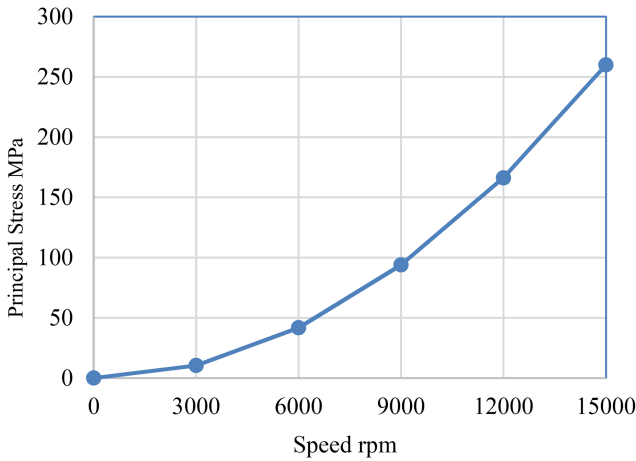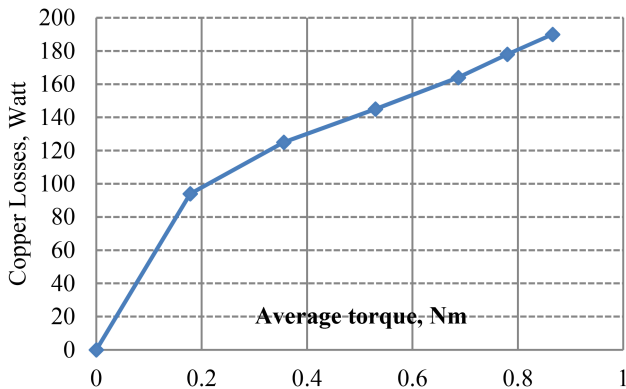
Fig. 22 *Stress verses speed*

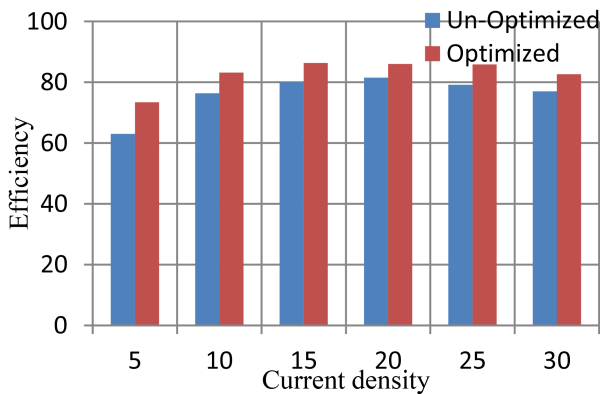**Fig. 23** *Copper losses versus average torque*

Fig. 24 *Efficiency versus armature current density(A/mm^2)*

8 Efficiency and loss analysis

Figs. 23 and 24, show the efficiency and copper losses of the proposed design 12-slot/13-pole outer rotor FEFSM. The copper losses are calculated from the (10).

$$P_c = \rho(2L + 2L_{end}) \times J \times I \times N \times N_{slot} \qquad (10)$$

Where L, L_{end}, and P_c are the stack length, estimated end coil length, and copper losses respectively, while N, J, N_{slot}, and I are number of turns, current density, number of stator slot, and current respectively and ρ is resistivity of copper, having $2.224 \times 10\text{-}8$ Ωm constant value. Fig. 23 shows the copper losses analysis of 12-slot/13-pole outer rotor FEFSM. The outer rotor FEFSM at the armature current density of 20 A/mm^2 and field current density of 20 A/mm^2 has 6.5 percent less copper losses as compared to 6-slot/7-pole WFFSM [19]. It is observed the increasing armature current density increases in copper losses too.

The copper losses of FEC and armature windings are analytically determined from their geometries, by taking into consideration the end coil effect. Furthermore, the iron losses including eddy current and hysteresis losses are calculated by 2D-FEA solver providing loss data sheet of 35H210 material.

Fig. 24 illustrates that efficiency bar of un optimized and optimized design versus armature current density J_a. Fig. 24 shows that at J_a 5A/mm^2, the efficiency is 73.4 percent which is lowest due to high speed of the machine and few copper losses because of less current density. The average efficiency of the machine is 82.90 percent. The average efficiency of both un-optimized and optimized machine is 76.175 percent and 82.90 percent respectively and 8.2 percent efficiency of optimized design greater than un-optimized design. The copper losses are calculated from (10). The highest efficiency of the machine is achieved at current density of 15 A/mm^2. At that point, the speed of the machine decreases causing less iron losses. On further increase in current density, the efficiency of the machine decreases due to high copper losses.

9 Conclusion

The performance and design analysis of three-phase outer rotor FEFSM employing salient rotor pole with seven different rotor pole topologies have been examined. The proposed design has novelty of outer rotor, non-overlapping winding, and robust rotor structure that reduced copper losses, gave low cost, high efficiency, and can be used for high-speed applications. The no load and load tests were executed to validate the efficacy of the proposed design.

The initial design achieved inadequate power and torque production. Therefore, a deterministic optimization technique was adopted to improve the characteristics. Moreover, FEA result was validated through MEC. Accuracy of nonlinear GRN and MEC models for 12slot/13pole outer rotor FEFSM was validated by comparing no-load U-phase flux linkage with corresponding result of FEA. This resulted in less than ~1.2% error. The optimized design enhanced power, torque, and efficiency compared to existing 6-slot/7-pole WFFSM.

10 References

[1] Emadi, A., Lee, Y.J., Rajashekara, K.: 'Power electronics and motor drives in electric, hybrid electric, and plug-in hybrid electric vehicles', *IEEE Trans. Ind. Electron.*, 2008, **55**, (6), pp. 2237–2245
[2] Chen, Y., Li, X., Wiet, C., *et al.*: 'Energy management and driving strategy for in-wheel motor electric ground vehicles with terrain profile preview', *IEEE Trans. Ind. Inf.*, 2014, **10**, (3), pp. 1938–1947
[3] Chung, S.U., Moon, S.H., Kim, D.J., *et al.*: 'Development of a 20-pole-24-slot SPMSM with consequent pole rotor for In-wheel direct drive', *IEEE Trans. Ind. Electron.*, 2016, **63**, (1), pp. 302–309
[4] Khan, F., Sulaiman, E., Ahmad, M.Z.: 'A novel wound field flux switching machine with salient pole rotor and nonoverlapping windings', *Turkish J. Electr. Eng. Comput. Sci.*, 2017, **25**, (2), pp. 950–964
[5] Zhu, Z.Q., Chan, C.C.: 'Electrical machine topologies and technologies for electric, hybrid, and fuel cell vehicles'. Vehicle Power and Propulsion Conf. VPPC'08 IEEE, Harbin, China, 2008, pp. 1–6
[6] Zhang, G., Hua, W., Cheng, M., *et al.*: 'Investigation of an improved hybrid-excitation flux-switching brushless machine for HEV/EV application', *IEEE Trans. Ind. Appl.*, 2015, **51**, (5), pp. 3791–3799
[7] Lee, C.H., Chau, K.T., Liu, C., *et al.*: 'Design and analysis of a magnet less flux-switching DC-excited machine for wind power generation', *J. Int. Council Electr. Eng.*, 2014, **4**, (1), pp. 80–87
[8] Zhou, Y.J., Zhu, Z.Q.: 'Comparison of low-cost single-phase wound-field switched-flux machines', *IEEE Trans. Ind. Appl.*, 2014, **50**, (5), pp. 3335–3345
[9] Khan, F., Sulaiman, E., Ahmad, M.Z.: 'Coil test analysis of wound-field three-phase flux switching machine with non-overlapping winding and salient rotor'. 2014 IEEE 8th Int. Power Engineering and Optimization Conf. (PEOCO), Langkawi, Malaysia, March 2014, pp. 243–247
[10] Tang, Y., Paulides, J.J., Lomonova, E.A.: 'Energy conversion in DC excited flux-switching machines', *IEEE Trans. Magn.*, 2014, **50**, (11), pp. 1–4
[11] Zulu, A., Mecrow, B.C., Armstrong, M.: 'A wound-field three-phase flux-switching synchronous motor with all excitation sources on the stator', *IEEE Trans. Ind. Appl.*, 2010, **46**, (6), pp. 2363–2371
[12] Zhu, Z.Q., Zhou, Y.J., Chen, J.T.: 'Electromagnetic performance of non-overlapping stator wound field synchronous machine with salient pole rotor', *IEEE Trans. Magn.*, 2015, **51**, (11), pp. 1–4
[13] Zhu, Z.Q., Zhou, Y.J., Chen, J.T., *et al.*: 'Investigation of nonoverlapping stator wound-field synchronous machines', *IEEE Trans. Energy Convers.*, 2015, **30**, (4), pp. 1420–1427

[14] Ahmad, N., Khan, F., Rashid, A.*, et al.*: 'Rotor pole study of outer rotor wound field flux switching motor for in wheel drive'. Int. Conf. on Computing, Mathematics and Engineering Technologies (iCoMET), Sukkur, Pakistan, 2018, pp. 1–5

[15] Othman, S.M.N.S., Jusoh, L.I.B., Hassan, M.K.*, et al.*: 'Rotor pole analysis for 12slot outer-rotor field excitation flux switching motor (ORFEFSM) for electric vehicle'. 2015 IEEE Student Conf. on Research and Development (SCOReD), Kuala Lumpur, Malaysia, December 2015, pp. 511–516

[16] Arbab, N., Wang, W., Lin, C.*, et al.*: 'Thermal modeling and analysis of a double-stator switched reluctance motor'. *IEEE Trans. Energy Convers.*, 2015, **30**, (3), pp. 1209–1217

[17] Tang, Y., Motoasca, T.E., Paulides, J.J.H.*, et al.*: 'Analytical modeling of flux-switching machines using variable global reluctance networks'. XXth Int. Conf. on Electrical Machines (ICEM), Marseille, France, September 2012, pp. 2792–2798

[18] Ostovic, V.: '*Dynamics of saturated electric machines*' (Springer-Verlag New York Inc., Berlin Heidelberg, Germany, 1989)

[19] Khan, F., Sulaiman, E., Ahmad, M.Z.: 'Review of switched flux wound-field machines technology'. *IETE Tech. Rev.*, 2017, **34**, (4), pp. 343–352